Vascular Endothelial Growth Factor–Mediated Islet Hypervascularization and Inflammation Contribute to Progressive Reduction of β-Cell Mass

Judith Agudo,[1,2,3] Eduard Ayuso,[1,2,3] Veronica Jimenez,[1,2,3] Alba Casellas,[1,2,3] Cristina Mallol,[1,2,3] Ariana Salavert,[1,2] Sabrina Tafuro,[1,2,3†] Mercè Obach,[1,2,3] Albert Ruzo,[1,2,3] Marta Moya,[1,2,3] Anna Pujol,[1,3] and Fatima Bosch[1,2,3]

Type 2 diabetes (T2D) results from insulin resistance and inadequate insulin secretion. Insulin resistance initially causes compensatory islet hyperplasia that progresses to islet disorganization and altered vascularization, inflammation, and, finally, decreased functional β-cell mass and hyperglycemia. The precise mechanism(s) underlying β-cell failure remain to be elucidated. In this study, we show that in insulin-resistant high-fat diet-fed mice, the enhanced islet vascularization and inflammation was parallel to an increased expression of vascular endothelial growth factor A (VEGF). To elucidate the role of VEGF in these processes, we have genetically engineered β-cells to overexpress VEGF (in transgenic mice or after adeno-associated viral vector-mediated gene transfer). We found that sustained increases in β-cell VEGF levels led to disorganized, hypervascularized, and fibrotic islets, progressive macrophage infiltration, and proinflammatory cytokine production, including tumor necrosis factor-α and interleukin-1β. This resulted in impaired insulin secretion, decreased β-cell mass, and hyperglycemia with age. These results indicate that sustained VEGF upregulation may participate in the initiation of a process leading to β-cell failure and further suggest that compensatory islet hyperplasia and hypervascularization may contribute to progressive inflammation and β-cell mass loss during T2D. ***Diabetes*** **61:2851–2861, 2012**

Type 2 diabetes (T2D) results from inadequate insulin secretion, which is unable to compensate for insulin resistance, due to the combination of decreased β-cell mass and function (1–3). Although defects in both insulin secretion and action contribute to the pathogenesis of T2D, it is now recognized that insulin deficiency is the critical constituent, without which T2D does not develop. As β-cell secretory capacity deteriorates, glucose tolerance worsens, eventually culminating in overt hyperglycemia (3). Post mortem studies revealed that type 2 diabetic patients have reduced β-cell mass and increased β-cell apoptosis rates (4,5). Loss of β-cell mass and function results from persistent hyperglycemia and hyperlipidemia, together with islet inflammation and increased proinflammatory cytokine production (6–9). However, the mechanisms underpinning increased β-cell death remain to be elucidated.

In the early stages of T2D, expansion of β-cell mass is a key adaptive response to compensate for insulin resistance (2). During this period, islet vasculature also needs to expand to perfuse the new β-cells (10). The formation of vessels in adult organisms (angiogenesis) occurs through a multistep process requiring vascular endothelial growth factor A (VEGF) and other soluble factors (11,12). VEGF recruits circulating monocytes and macrophages, which are required for active angiogenesis (13). In adults, VEGF is highly expressed and secreted by insulin-producing β-cells and is responsible for the rich islet vascularization (14–16). VEGF deficiency in β-cells does not modify β-cell mass, but leads to insufficient islet vascularization, which results in defective insulin secretion and glucose intolerance (14,17). However, this deficiency does not impair β-cell mass growth during a high-fat diet (HFD); contrarily, it results in a slightly increased β-cell mass (18). Furthermore, islet vascular abnormalities have been described in several animal models of T2D. Prior to developing hyperglycemia, islets from Zucker diabetic fatty rats show vessel remodeling with expansion of endothelial cells and higher VEGF secretion (19). Similarly, pancreatic islets from spontaneously diabetic Torii rats are fibrotic with vascular alterations preceding hyperglycemia (20). Goto-Kakizaki (GK) rats also show endothelial hypertrophy with increased expression of vessel extracellular matrix components (21), and Otsuka Long-Evans Tokushima fatty rats display fibrosis and vascular abnormalities in islets (22). Finally, *db/db* mice develop irregular vessels with increased mean capillary size, edema, and fibrosis (23). In mouse islets, endothelial cells synthesize extracellular matrix (ECM) components surrounding β-cells (24–26). ECM accumulation surrounding islet vessels in T2D models can progress to fibrosis that disrupts islet structure (21). Taken together, these studies suggest that alterations in islet vasculature may precede and/or be involved in β-cell dysfunction and death. Nevertheless, the role of chronic islet hypervascularization in β-cell function and loss in T2D is still not fully understood. In this study, by genetically engineering β-cells to overexpress VEGF, we demonstrate that sustained increases in VEGF levels leads to islet hypervascularization, fibrosis, and inflammation, resulting in β-cell death and hyperglycemia.

RESEARCH DESIGN AND METHODS

Animals. C57Bl6/SJL transgenic mice expressing murine $VEGF_{164}$ (provided by P.A. D'Amore, Boston, MA) under the control of the rat insulin promoter-I

From the [1]Center of Animal Biotechnology and Gene Therapy, Universitat Autònoma de Barcelona, Barcelona, Spain; the [2]Department of Biochemistry and Molecular Biology, Universitat Autònoma de Barcelona, Barcelona, Spain; and the [3]Centro de Investigación Biomédica en Red de Diabetes y Enfermedades Metabólicas Asociadas, Barcelona, Spain.
Corresponding author: Fatima Bosch, fatima.bosch@uab.es.
Received 8 February 2012 and accepted 29 May 2012.
DOI: 10.2337/db12-0134
This article contains Supplementary Data online at http://diabetes.diabetesjournals.org/lookup/suppl/doi:10.2337/db12-0134/-/DC1.
†Deceased.
E.A. and V.J. contributed equally to this work.

(RIP-I) were obtained by embryo pronuclear microinjection. Both $VEGF^{low}$ and $VEGF^{high}$ transgenic mice were born at the expected frequencies and fertile, and they did not develop tumors when old (>14 months). Two-month-old C57Bl6/SJL mice were used for adeno-associated viral (AAV) vector treatment. Diabetes was assessed by measuring tail vein blood glucose levels using a Glucometer Elite analyzer (Bayer). Mice were fed ad libitum with a standard chow diet (Basal Purified Diet with 12% energy from fat) or an HFD (Basal Purified Diet with 60% energy from fat, TD.88137; Harlan Teklad). In all experiments, male mice were age-matched. Animal care and experimental procedures were approved by the Ethics Committee in Animal and Human Experimentation of the Universitat Autònoma de Barcelona.

VEGF and insulin determinations. VEGF levels in serum and islet homogenates were measured by ELISA (Calbiochem, Nothingam, U.K.). Insulin levels in serum were determined by radioimmunoassay (Linco, St. Charles, MO).

Immunohistochemical analysis. Pancreata were fixed for 24 h in formalin, embedded in paraffin, and sectioned. For immunohistochemical detection of insulin, glucagon, VEGF-A, CD31, Mac-2, and glucose transporter (GLUT)-2, pancreatic sections were incubated overnight at 4°C with a guinea pig anti-insulin antibody (Sigma Chemical, St. Louis, MO), a rabbit antiglucagon antibody (ICN Biomedicals Inc.), a mouse anti–VEGF-A antibody (Santa Cruz Biochemicals), a rat anti-mouse CD31 antibody (BD Biosciences), a rabbit anti–Mac-2 antibody (Cedarlane Laboratories), or a rabbit anti–GLUT-2 antibody (Chemicon International, Temecula, CA). Secondary antibodies were: tetramethyl rhodamine isothiocyanate-conjugated goat anti-guinea pig (Molecular Probes, Leiden, the Netherlands); biotinylated goat anti-rabbit (Molecular Probes); biotinylated donkey anti-goat (Santa Cruz Biotechnology); biotinylated rabbit anti-rat (DakoCytomation, Glostrup, Denmark); biotinylated goat anti-rabbit (Molecular Probes); biotinylated horse anti-mouse (Vector Laboratories, Burlingame, CA); streptavidin-conjugated Alexa 488 (Molecular Probes); or streptavidin-conjugated Alexa 568 (Molecular Probes). For anti-mouse antibody detection, M.O.M kit (Vector Laboratories) was used. Nuclei were counterstained with Hoechst (Sigma-Aldrich). Bright field sections were counterstained with hematoxylin.

Fluorescein-dextran injection. To visualize vessels within the islets, a dextran–fluorescein isothiocyanate (FITC) solution (Sigma-Aldrich; 50 mg/mL PBS) was administered by tail vein injection. After 10 min, animals were sacrificed, and pancreata were fixed for 12–24 h in formalin, embedded in paraffin, and sectioned.

Morphometrical analysis. For morphometrical analysis of β-cell mass, immunohistochemical detection of insulin was performed in three (2 to 3 μm) sections, separated by 200 μm in each animal. The percentage of β-cell area in the pancreas was calculated by dividing the area of all insulin-positive cells in one section by the total area of this section and multiplying the result by 100. The β-cell mass was calculated by multiplying the pancreas weight by the percent of β-cell area. For measurement of β-cell proliferation, replicating β-cells were identified by double Ki67/insulin immunostaining. Apoptotic β-cells were determined by double transferase-mediated dUTP nick-end labeling (TUNEL)/insulin immunostaining. At least 5,000 β-cells per pancreas were counted. Four animals per group were used in each analysis. For morphometrical analysis of islet vascularization, FITC-positive area and insulin-positive area were determined in pancreatic sections from FITC-conjugated dextran-injected animals. Macrophage infiltration was measured as the percentage of Mac-2–positive area per islet area. Islet vascularization and macrophage infiltration were quantified by measuring islets from three different sections per mouse, with four animals per group. A microscope (Eclipse E800; Nikon, Tokyo, Japan) connected to an image analyzer was used. For laser-scanning confocal analysis, a TCS SP2 microscope (Leica Microsystems, Heidelberg, Germany) was used.

Isolation of islets. Pancreatic islets were isolated by intraductal injection of collagenase solution (1 mg/mL collagenase P; Roche Molecular Biochemicals, Mannheim, Germany) and digestion in Hanks' balanced salt solution (HBSS) containing 1% BSA and 5 mmol/L glucose for 10 min at 37°C. Cold HBSS (with 1% BSA and 5 mmol/L glucose) was added to stop the digestion. The tissue suspension was washed twice with cold HBSS. Islets were handpicked.

Gene expression analysis. For quantitative RT-PCR analysis, total RNA was extracted from isolated islets using Tripure Isolation Reagent (Roche Molecular Biochemicals) and RNeasy Mini Kits (Qiagen, Hilden, Germany). Total RNA (1 μg) was reverse-transcribed for 1 h at 37°C using the Omniscript Reverse transcriptase kit (D-40724; Qiagen). Quantitative PCR (qPCR) was performed in a SmartCycler II (Cepheid, Sunnyvale, CA) using the Quantitect SYBR green kit (Qiagen).

For gene expression analysis, the following primers were used: interleukin-1β (IL-1β) forward, 5′-CAACCAACAAGTGATATTCTCCATG-3′ and reverse, 5′-CATCCACACTCTCCAGCTGCA-3′; tumor necrosis factor-α (TNF-α) forward, 5′-CATCTTCTCAAAATTCGAGTGACAA-3′ and reverse 5′-TGGGAGTAGACAAGGTACAACCC-3′; CCL-2 forward, 5′-CCCAATGAGTAGGCTGGAGA-3′ and reverse, 5′-TCTGGACCCATTCCTTCTTG-3′; IL-6 forward, 5′-AGTTGCCTTCTTGGGACTGA-3′ and reverse, 5′-TCCACGATTTCCCAGAGAAC-3′; RBS forward, 5′-ATTCGCTGCACGAACTGCG-3′ and reverse, 5′-CAGCAGGTCTGAATCGTGGT-3′; and GLUT-2 forward, 5′-CTGGAGCCCTCTTGATGGGA-3′ and reverse, 5′-CCAGTCCTGAAATTAGCCCAC-3′.

Western blot analysis. Isolated islets were homogenized in protein lysis buffer after being washed with PBS. Proteins (50–100 μg) were separated by 10% SDS-PAGE, transferred to polyvinylidene difluoride membranes, and probed with primary antibodies against VEGF (Abcam), E-cadherin (Santa Cruz Biotechnology), and β-actin (Abcam) overnight at 4°C. Detection was performed using horseradish peroxidase-labeled anti-goat immunoglobulin G or horseradish peroxidase-labeled anti-rabbit immunoglobulin G (DakoCytomation) and ECL Plus Western Blotting Detection Reagent (Amersham Biosciences). Data were obtained from three pools of islets and four mice per pool.

Recombinant AAV vectors. Vectors were generated by triple transfection of human embryonic kidney 293 cells. Cells were cotransfected with a plasmid carrying the expression cassette, a helper plasmid carrying the AAV *rep2* and *cap9* genes, and a plasmid carrying the adenovirus helper functions (provided by K.A. High, Children's Hospital of Philadelphia). The transgene used in these experiments was murine $VEGF_{164}$ under the control of RIP-I promoter followed by woodchuck hepatitis virus posttranscriptional regulatory element sequence to increase expression. AAV null vectors were produced using pAAV-MCS plasmid (Stratagene, La Jolla, CA). Vectors were purified with an optimized method using cesium chloride gradients (27), dialyzed, filtered, titred by qPCR, and stored at −80°C until use.

In vivo administration of AAV. Mice were anesthetized with an intraperitoneal injection of ketamine (100 mg/kg) and xylazine (10 mg/kg). A microclamp was placed on the bile duct caudal to the liver to prevent vector distribution. A 30-gauge needle was used to advance retrogradially through the sphincter of Oddi into the common bile duct. A volume of 100 μL of AAV vectors diluted in PBS was injected into the duct. A dose of 10^{12} vector genomes per mouse was used.

Statistical analysis. All values are expressed as the means ± SEM. Differences between groups were compared by Student *t* test. A P value <0.05 was considered statistically significant.

RESULTS

Increased islet vascularization and inflammation parallels enhanced VEGF production in type 2 prediabetic mice. Islet vascularization and VEGF expression were determined in 6-month-old C57Bl6 mice fed with an HFD for 4 months. HFD-fed mice developed insulin resistance, as they were normoglycemic (chow, 136 ± 13.5 vs. HFD, 143 ± 17.5 mg/dL) and highly hyperinsulinemic (chow, 2.3 ± 0.4 vs. HFD, 8.1 ± 1.7 ng/mL) and showed altered insulin tolerance (Supplementary Fig. 1). In contrast to mice fed a chow diet, islets from HFD-fed mice were larger (chow, 290 ± 65 vs. HFD, 435 ± 110 μm^2; $P < 0.05$), indicating compensatory islet hyperplasia. Islets from these mice showed hypervascularization with thicker basal membranes after staining for the endothelial cell marker CD31 and the basement membrane marker collagen IV (Fig. 1*A* and *B*). To investigate whether intraislet vasculature was functional, a FITC-conjugated dextran solution was intravenously injected in these mice. An increased vessel area/islet area ratio (~25%) was observed in HFD-fed mice, indicating higher islet vascularization (Fig. 1*C* and *D*). This suggests that in hyperplasic islets, angiogenesis might have increased to perfuse new β-cells. This was parallel to the increased VEGF content (about twofold) in HFD islets (Fig. 1*E* and *F*). Because VEGF can induce collagen IV synthesis by endothelial cells (28), VEGF upregulation was probably responsible for the increased amount of endothelial ECM of these islets (Fig. 1*A*). Because fibrosis and VEGF upregulation are also usually found during inflammatory processes (11), pancreatic sections were stained for the macrophage cell marker Mac-2, and an increase in macrophage infiltration in the islets of HFD-induced insulin resistant mice was

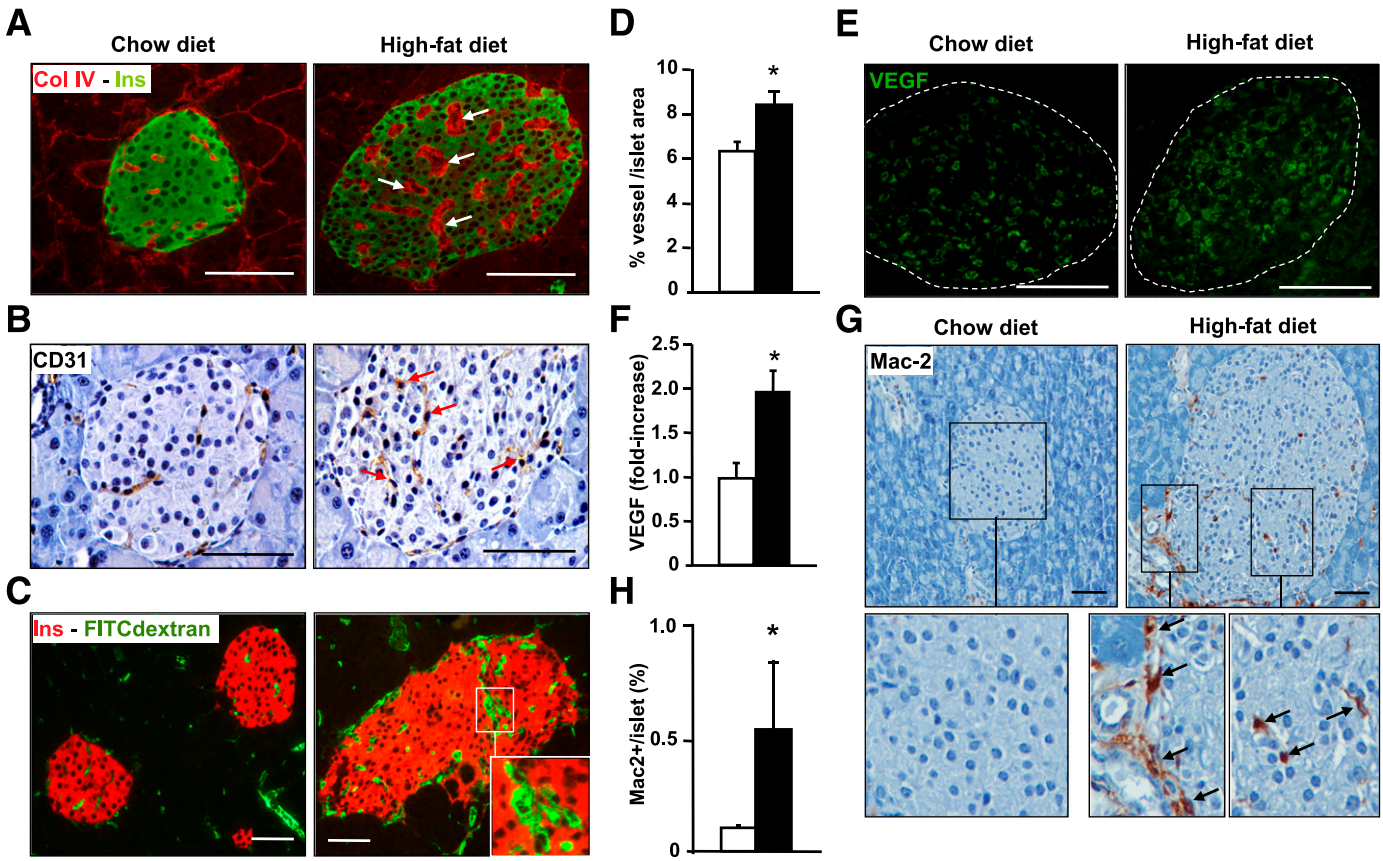

FIG. 1. Hypervascularization and macrophage infiltration in pancreatic islets from insulin-resistant HFD-fed mice. *A*: Islet vessels were revealed by dual collagen IV (red) and insulin (green) immunostaining. Arrows point to thickened basement membrane. *B*: Endothelial cells were immunostained by CD31 antibody. HFD-fed mice showed more endothelial cells per islet (arrows). *C*: Pancreatic sections from HFD- and chow-fed FITC-dextran–infused mice showing vessels (green) and insulin (red). Capillaries with a large lumen are shown in the inset. *D*: HFD animals (black bar) showed increased FITC-dextran area/islet area compared with chow-fed mice (white bar) (n = 3/group). *P < 0.05 HFD vs. chow diet. *E*: VEGF immunostaining of pancreatic sections from HFD- and chow-fed mice. *F*: VEGF content in protein extracts of isolated islets from individual animals chow-fed mice (white bar) and HFD mice (black bar) was determined by ELISA (n = 4/group). HFD mice displayed a marked increase in Mac-2–positive macrophage infiltration in islets as shown after immunohistochemical analysis (*G*) and morphometrical analysis (*H*) (chow-fed mice [white bar] and HFD mice [black bar]). Infiltrating macrophages at the periphery and inside the islet are shown in the inset (arrows) (n = 3/group). Scale bars, 100 μm. *P < 0.05 HFD vs. chow. (A high-quality digital representation of this figure is available in the online issue.)

observed (Fig. 1*G* and *H*). These results suggest that insulin resistance induces compensatory islet hyperplasia together with increased islet VEGF expression, angiogenesis, and macrophage recruitment.

VEGF overexpression in islets leads to hypervascularization, altered morphology, and inflammation. To elucidate the role of VEGF in islet angiogenesis and β-cell function, transgenic mice overexpressing VEGF in β-cells under the control of the RIP-I were generated. Two transgenic lines, VEGF^{low} and VEGF^{high}, with a 2.7- and 17-fold increase in VEGF expression (Fig. 2*A* and *B*), respectively, were obtained. VEGF^{low} mice showed an increase in VEGF comparable to that observed in insulin-resistant mice (Fig. 1*F*) and rats (19). VEGF serum concentrations remained unchanged (wild-type, 221 ± 27.8; VEGF^{low}, 202 ± 29.3; and VEGF^{high}, 189 ± 25.1 ng/dL), suggesting an autocrine/paracrine effect of VEGF in the pancreas. Compared with wild-type, 2-month-old VEGF^{low} and VEGF^{high} islets displayed hypervascularization and basal membrane thickening, as shown by both CD31 and collagen IV immunostaining (Fig. 2*C*). Intravascular injection of FITC-conjugated dextran confirmed the increased vessel area/islet area ratio of functional capillaries (Fig. 2*C* and *D*).

Islets from 2-month-old VEGF^{low} and VEGF^{high} mice showed altered distribution of α and β-cells (Fig. 3*A*). Although the basal membrane of islet endothelial cells provides signals that promote β-cell proliferation (15) and transgenic islets were hypervascularized, the β-cell mass was similar in wild-type, VEGF^{low}, and VEGF^{high} mice (Fig. 3*B*). This was consistent with normal rates of β-cell replication and apoptosis (Fig. 3*C–F*). This altered islet morphology was parallel to decreased levels of E-cadherin (Fig. 3*F* and *G*), a key protein in maintaining islet endocrine cell contacts (29,30).

Long-term β-cell overexpression of VEGF leads to glucose intolerance and hyperglycemia. Two-month-old wild-type, VEGF^{low}, and VEGF^{high} mice presented similar glycemia, insulinemia (Fig. 4*A* and *B*), and glucose tolerance (Fig. 4*C*). In addition, comparable in vivo insulin secretion profiles were noted in all groups (Fig. 4*D*). This was consistent with normal GLUT-2 expression in VEGF^{low} islets (Fig. 4*E* and *F*). However, VEGF^{high} islets showed a decrease in GLUT-2 expression without a major change in insulin secretion (Fig. 4*E* and *F*). Therefore, although transgenic islets were disorganized and hypervascularized, glucose homeostasis in young transgenic mice was nevertheless unaltered, indicating normal islet function, in agreement with the normal β-cell mass.

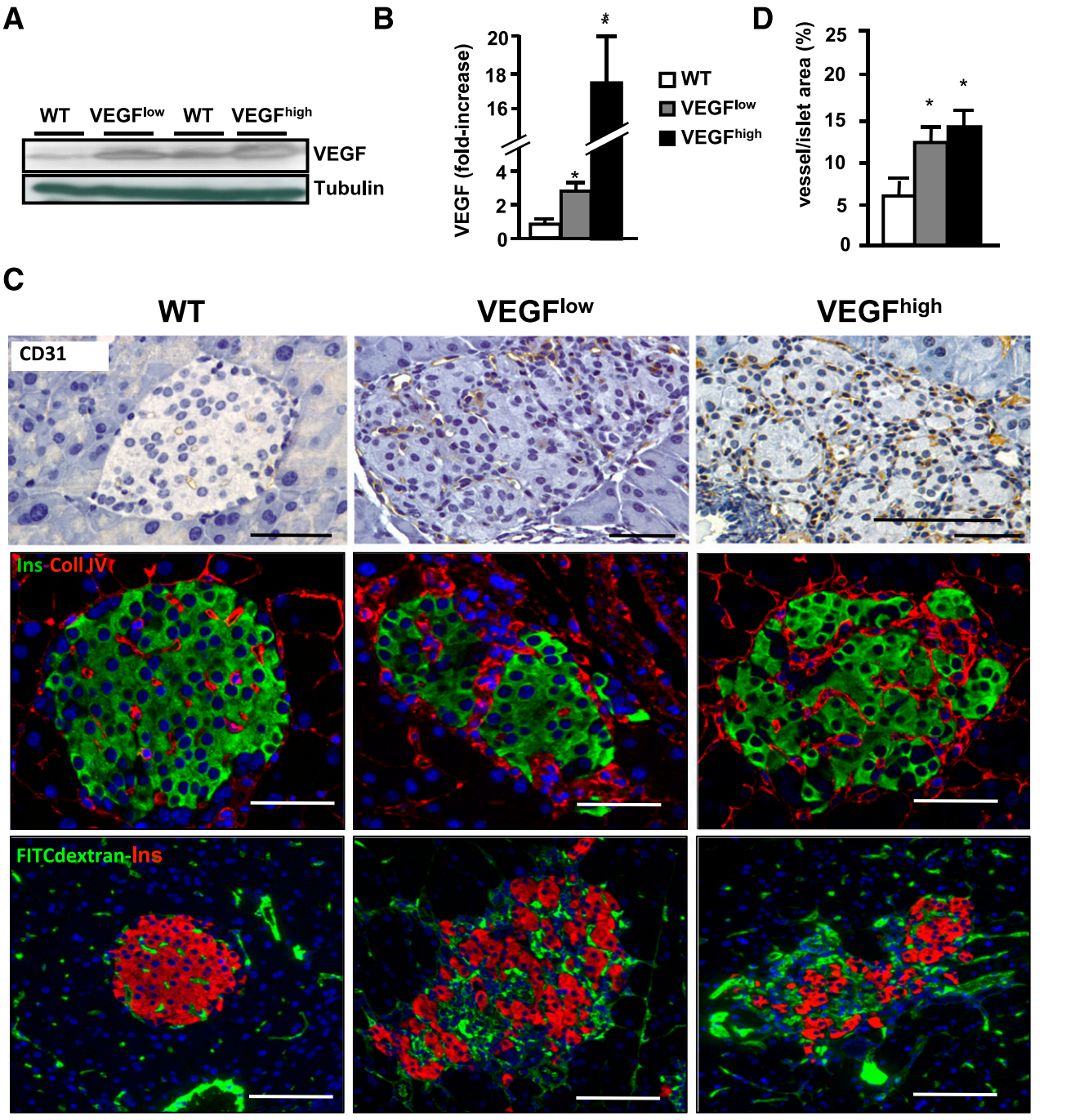

FIG. 2. Increased VEGF expression in VEGF^{low} and VEGF^{high} transgenic β-cells leads to islet hypervascularization. *A*: Representative Western blot showing higher expression of VEGF in both VEGF^{high} and VEGF^{low}. *B*: A 2.7- and 17-fold increase in VEGF protein levels were found in islets from 2-month-old VEGF^{low} and VEGF^{high} mice measured by ELISA, wild-type (WT) mice (white bar), transgenic VEGF^{low} mice (gray bar), and transgenic VEGF^{high} mice (black bar). *P < 0.05 transgenic vs. WT (n = 8–15/group). *C*: *Top panel*: detection of endothelial cells by CD31 immunostaining. *Middle panel*: collagen IV (red) and insulin (green) immunohistochemical analysis of VEGF^{low} and VEGF^{high} islets. *Bottom panel*: FITC-dextran (green) together with insulin (red) immunostaining was used to label functional islet vessels. *D*: Morphometric analysis revealed an increase in the vessel area in both VEGF^{low} and VEGF^{high} mice (n = 3/group): WT mice (white bar), transgenic VEGF^{low} mice (gray bar), and transgenic VEGF^{high} mice (black bar). Scale bars, 100 μm. *P < 0.05 transgenic vs. WT. (A high-quality digital representation of this figure is available in the online issue.)

VEGF^{low} mice remained normoglycemic up to 12 months of age, when they developed mild hyperglycemia and hypoinsulinemia (Fig. 4*A* and *B*), altered glucose tolerance, and decreased glucose-stimulated insulin release (Fig. 5*A* and *B*), but normal insulin sensitivity (data not shown). In contrast, VEGF^{high} mice, which expressed higher VEGF levels, developed glucose intolerance and decreased insulin secretion after a glucose load earlier, at 5 to 6 months of age (Fig. 5*C* and *D*). Moreover, 8-month-old VEGF^{high} mice displayed overt hyperglycemia, hypoinsulinemia (Fig. 4*A* and *B*), and glucose intolerance (Fig. 5*E*).

Morphometric analysis of pancreatic sections from VEGF^{low} mice showed a trend toward decreased β-cell mass only at the age of 12 months (Fig. 5*F* and *G*), although this

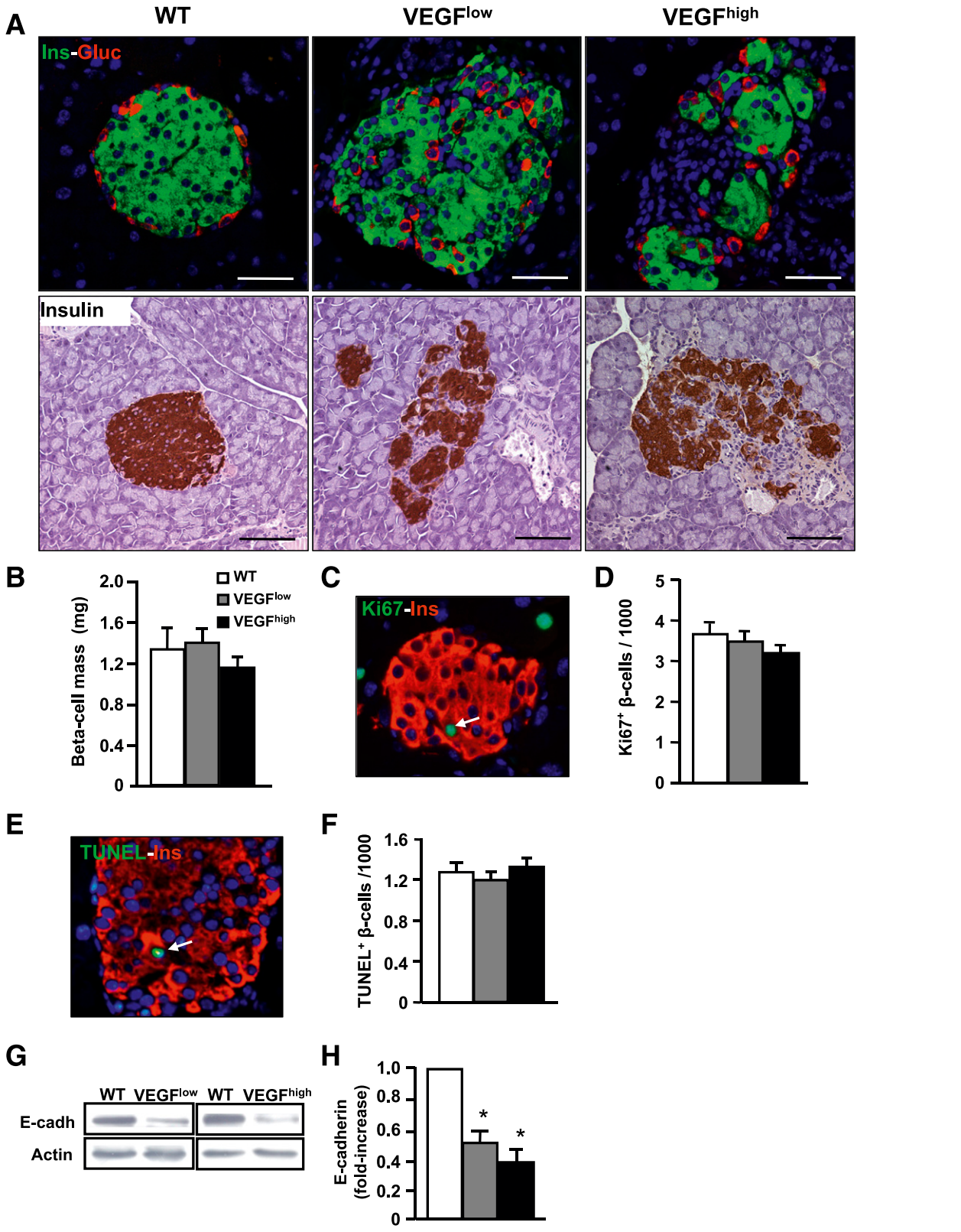

FIG. 3. Two-month-old VEGF^{low} and VEGF^{high} mice showed disorganization of islet architecture, but normal β-cell mass. *A*: *Top panel*: immunohistochemical analysis of insulin (green) and glucagon (red). In transgenic mice, islets appeared disorganized with α-cells in the core. *Bottom panel*: insulin immunostaining used to visualize islet architecture. *B*: β-Cell mass was measured in 2-month-old mice (n = 4–7/group): wild-type (WT) mice (white bar), transgenic VEGF^{low} mice (gray bar), and transgenic VEGF^{high} mice (black bar). *C*: Ki67 (green) and insulin (red) immunostaining were used to label proliferating β-cells (arrow). *D*: Percentage of Ki67-positive (replicative) β-cells. *E*: TUNEL (green) and insulin (red) immunostaining showed apoptotic nuclei (arrow). *F*: Quantification of TUNEL-positive (apoptotic) β-cells. *G* and *H*: Western blot analysis of E-cadherin using islet homogenates from 2-month-old mice. *G*: A representative immunoblot is shown. *H*: Densitometric analysis of three different immunoblots: WT mice (white bar), transgenic VEGF^{low} mice (gray bar), and transgenic VEGF^{high} mice (black bar). Scale bars, 100 μm. *P < 0.05 transgenic vs. WT. (A high-quality digital representation of this figure is available in the online issue.)

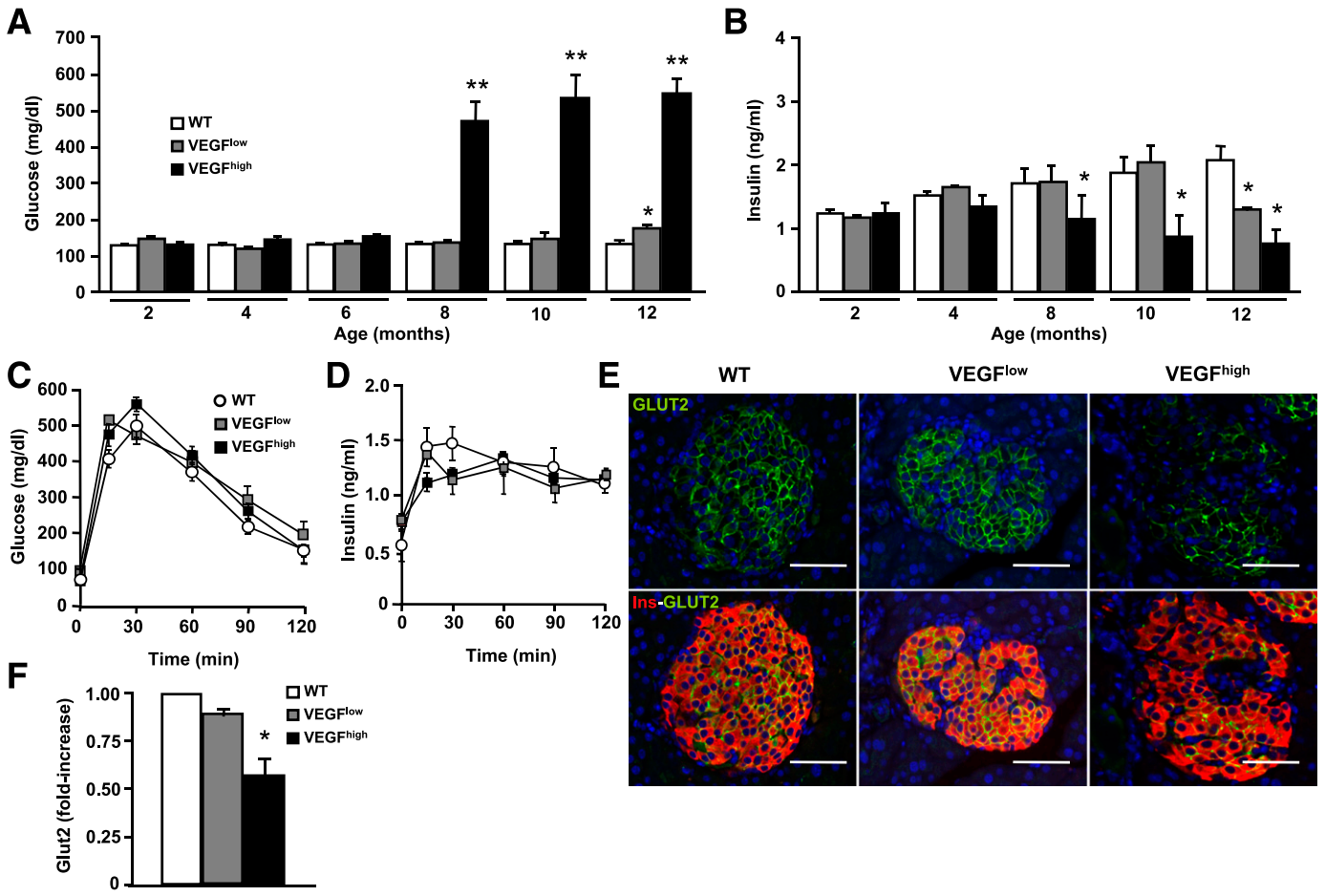

FIG. 4. Glucose homeostasis in VEGF^{low} and VEGF^{high} mice. Blood glucose (*A*) and insulin (*B*) levels were monitored in fed mice from 2–12 months: wild-type (WT) mice (white bar), transgenic VEGF^{low} mice (gray bar), and transgenic VEGF^{high} mice (black bar) (n = 15 animals/group). **P < 0.01 *P < 0.05 transgenic vs. WT. Glucose tolerance (*C*) and in vivo insulin secretion (*D*) were determined after an intraperitoneal glucose injection (2 g/kg body weight) into 2-month-old mice WT (white circle), VEGF^{low} mice (gray square), and VEGF^{high} mice (black square) (n = 10 animals/group). *E*: Immunohistochemical analysis of GLUT-2 (green) and insulin (red) in islets from 2-month-old mice is shown. *F*: GLUT-2 mRNA expression from isolated islets from 2-month-old VEGF^{low} and VEGF^{high} mice was determined by qPCR (n = 3 pools of islets from three mice per pool): WT mice (white bar), transgenic VEGF^{low} mice (gray bar), and transgenic VEGF^{high} mice (black bar). Scale bars, 100 μm. *P < 0.05 vs. WT mice. (A high-quality digital representation of this figure is available in the online issue.)

did not reach statistical significance (P = 0.059). In contrast, 8-month-old VEGF^{high} mice displayed a marked loss of β-cell mass (~80%) (Fig. 5*F* and *G*). In VEGF^{high} pancreata, insulin- and glucagon-positive cells were scattered and surrounded by abundant collagen IV-positive staining (Fig. 5*F*).

VEGF overexpression leads to islet inflammation and increased cytokine production. In addition to promoting angiogenesis, VEGF is involved in macrophage recruitment (13). Mac-2–positive cells were detected in islets from 2- to 12-month-old VEGF mice (Fig. 6*A* and *B*). Macrophage infiltration progressively increased as animals aged and in parallel with VEGF expression, being higher in VEGF^{high} than in VEGF^{low} islets (Fig. 6*A* and *B*). These results suggest that chronic overexpression of VEGF progressively increased macrophage recruitment. Consistent with this, a statistically significant increase in the expression of CCL-2 (monocyte chemoattractant protein-1), IL-1β, and TNF-α was observed in islets of 12-month-old VEGF^{low} mice and 5-month-old VEGF^{high} mice, although a tendency toward increased expression was already noted in 2-month-old mice (Fig. 6*C*–*E*). Thus, the development of hyperglycemia and decrease in β-cell mass were concomitant with progressive macrophage infiltration, cytokine production, and fibrosis.

In vivo AAV-mediated VEGF overexpression in β-cells of adult mice results in islet hypervascularization and inflammation. To avoid potentially undesirable effects of VEGF overexpression during embryonic development and to verify a direct effect of VEGF in endocrine pancreas inflammation, AAV vectors were used to overexpress VEGF in islets of adult mice. Intraductal delivery of AAV vectors of serotype 9 (AAV9) leads to highly efficient and long-term transduction of β-cells and exocrine pancreas (31). To restrict transgene expression to β-cells, the RIP-I promoter was used. Thus, AAV9 vectors carrying a RIP-I/VEGF transgene were intraductally injected into 2-month-old mice, and glucose homeostasis and islet morphology were studied within 2 months after AAV injection. Compared with AAV9-null–treated mice, AAV9-VEGF–treated animals showed about a twofold increase (AAV9-VEGF: 2.2 ± 0.8-fold increase vs. AAV9-null) in islet content of VEGF, similar to the increases detected in islets from HFD-fed mice, VEGF^{low} transgenic mice, or Zucker rats (19). This value was, however, variable among mice paralleling

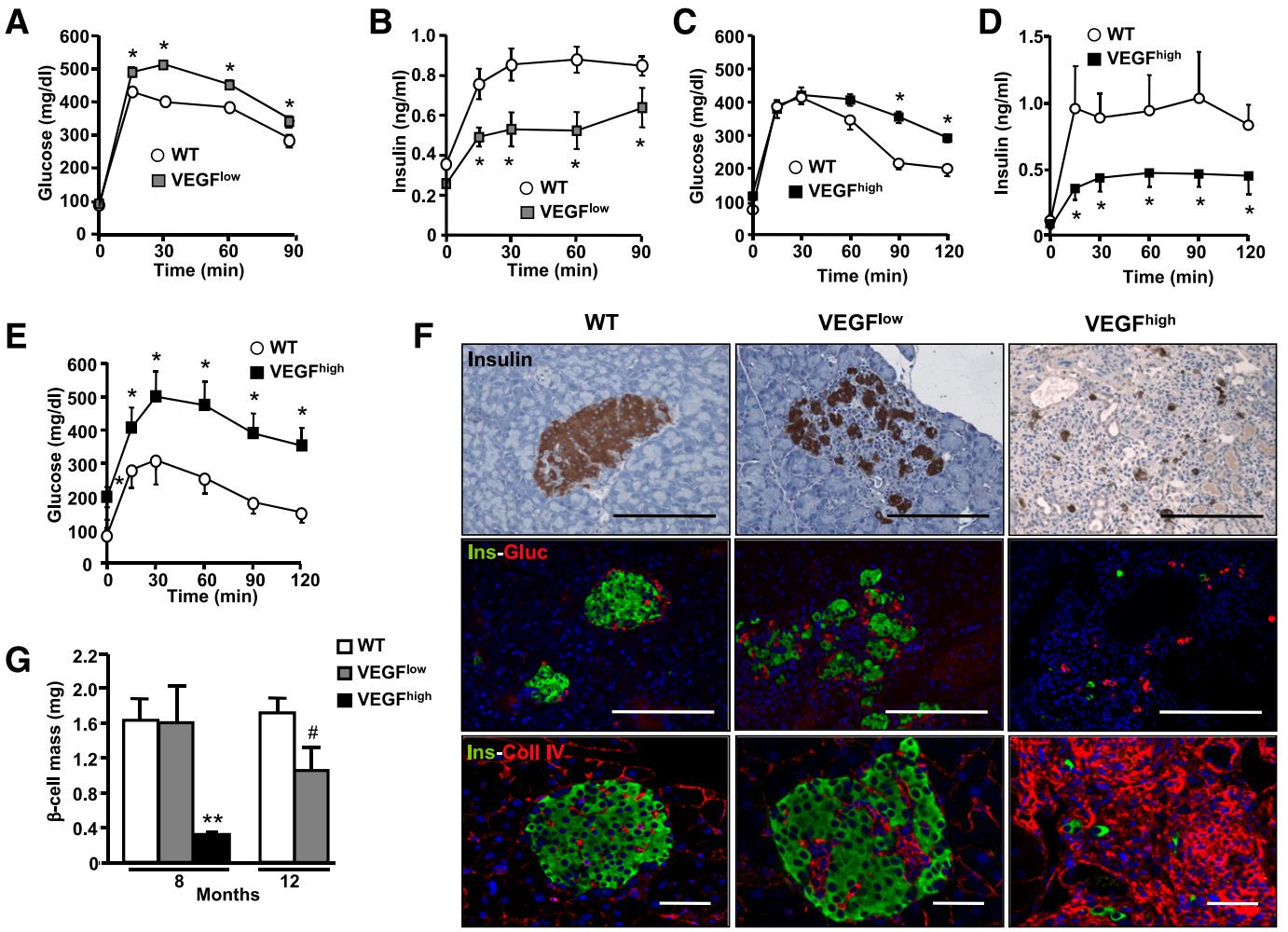

FIG. 5. Glucose homeostasis in VEGF^{low} and VEGF^{high} mice was impaired with age. Glucose tolerance (*A*) and insulin in vivo secretion (*B*) were measured in 12-month-old wild-type (WT) (white circle) and VEGF^{low} mice (gray square) (n = 12 animals/group). *P < 0.05 VEGF^{low} vs. WT mice. Glucose tolerance (*C*) was determined in parallel to in vivo insulin secretion (*D*) after a glucose load (2 g/kg body weight [b.w.]) in 5-month-old WT mice (white circle) and transgenic VEGF^{high} mice (black square). At this age, VEGF^{high} mice were normoglycemic, but showed impaired insulin release and glucose intolerance after the glucose load (n = 12 animals/group). *P < 0.05 VEGF^{high} vs. WT mice. *E*: Eight-month-old VEGF^{high} mice (black square) were glucose-intolerant compared with age-matched WT (white square) mice as shown by a glucose tolerance test (1 g/kg b.w.) (n = 10 animals/group). *P < 0.05 VEGF^{high} vs. WT mice. *F*: *Top panel*: representative images of insulin immunostaining of islets. *Middle panel*: immunohistochemical analysis of insulin (green) and glucagon (red) expression. *Bottom panel*: immunohistochemical analysis of collagen IV (red) and insulin (green). Islets from 12-month-old WT and VEGF^{low} and 8-month-old VEGF^{high} mice are shown. Scale bars, 100 μm. *G*: β-Cell mass was determined by insulin immunostaining in 8- and 12-month-old VEGF^{low} and 8-month-old VEGF^{high} mice and compared with age-matched WT mice, as indicated in RESEARCH DESIGN AND METHODS (WT mice [white bar], transgenic VEGF^{low} mice [gray bar], and transgenic VEGF^{high} mice [black bar]) (n = 3 sections/mouse and 4 animals/group). **P < 0.001 VEGF^{high} vs. WT mice, $^{\#}P$ < 0.1 VEGF^{low} vs. WT. (A high-quality digital representation of this figure is available in the online issue.)

differential efficiency of transduction. Despite the heterogeneity, all AAV9-VEGF–treated mice showed between 30 and 80% hypervascularized and disorganized islets, with increased collagen IV accumulation (Fig. 7*A*). These alterations were already observed 10 days after vector administration (Fig. 7*A*) and were also present at 40 days (Supplementary Fig. 2). Islet inflammation, determined by Mac-2 immunostaining, was increased in AAV9-VEGF–treated mice at 10 (Fig. 7*A* and *B*) and 40 days (Supplementary Fig. 2) after AAV injection. Moreover, increased VEGF expression in β-cells induced a progressive increase in glycemia (Fig. 7*C*), along with glucose intolerance (Fig. 7*D*). Thus, these results confirm that VEGF overexpression in islets of adult mice can induce hypervascularization, islet disorganization, and inflammation that result in impaired glucose homeostasis.

DISCUSSION

In the preliminary stages of T2D, expansion of β-cell mass is a key adaptive response to compensate for insulin resistance (2). During this period, islet vasculature also needs to expand to perfuse the newly formed β-cells. The development of vessels in adult organisms (angiogenesis) occurs through a multistep process requiring VEGF and other soluble factors (32). In this study, we found that islets from obese, insulin-resistant, HFD-fed mice displayed increased vascularization that paralleled increased VEGF levels. Similar observations were described in insulin-resistant prediabetic Zucker rats (32), in which islets of these rats showed increased vascularization and enhanced VEGF secretion compared with non–insulin-resistant rats. This may indicate that VEGF upregulation represents a compensatory response to support angiogenesis during β-cell

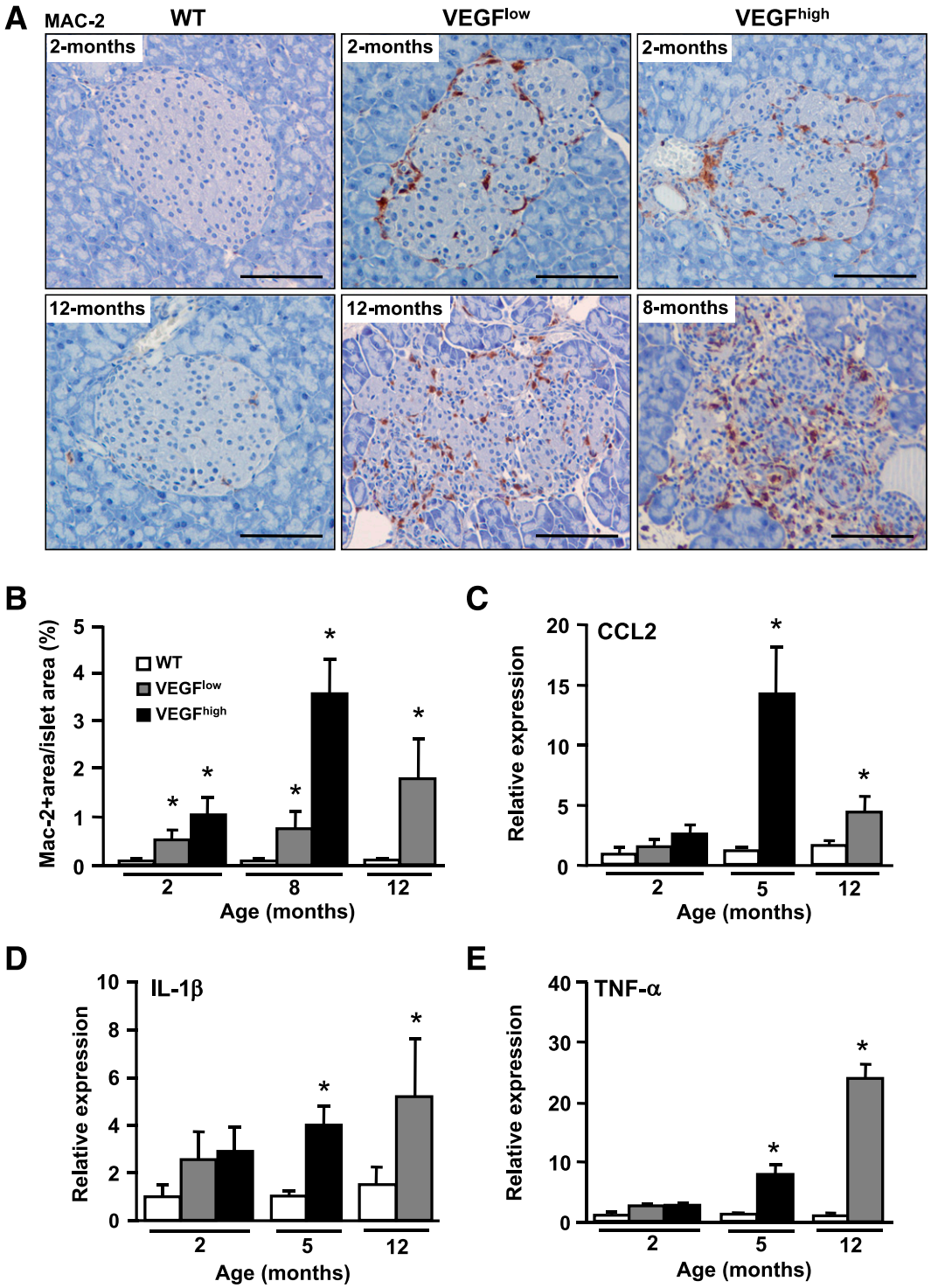

FIG. 6. VEGF-overexpressing islets showed progressive inflammation. *A*: Macrophage infiltration was determined by Mac-2 immunostaining in islets from 2-month-old wild-type (WT), VEGF^{low}, and VEGF^{high} mice (*top panel*) and 12-month-old WT and VEGF^{low} and 8-month-old VEGF^{high} mice (*bottom panel*). *B*: Quantification of Mac-2–positive area in pancreas sections from 2-, 8-, and 12-month-old WT, in 2-, 8-, and 12-month-old VEGF^{low}, and in 2- and 8-month-old VEGF^{high} mice (n = 4 animals/group): WT mice (white bar), transgenic VEGF^{low} mice (gray bar), and transgenic VEGF^{high} mice (black bar). *C–E*: Islets from VEGF^{low} and VEGF^{high} mice displayed increased expression of key inflammatory cytokines. CCL-2 (*C*), IL-1β (*D*), and TNF-α (*E*) were measured by qPCR from isolated islets from 2- and 12-month-old VEGF^{low} and 2- and 5-month-old VEGF^{high} mice (n = 4 pools of islets from three mice per pool): WT mice (white bar), transgenic VEGF^{low} mice (gray bar), and transgenic VEGF^{high} mice (black bar). Scale bars, 100 μm. *P < 0.05 vs. age-matched WT mice. (A high-quality digital representation of this figure is available in the online issue.)

expansion. To discern the role of increased VEGF and islet vascularization during T2D development, VEGF^{low} and VEGF^{high} transgenic mice were generated. Similar to HFD-fed mice, VEGF^{low} and VEGF^{high} mice displayed islet hypervascularization with irregular capillaries and thicker basal membranes. These vascular alterations resembled those observed in islets from HFD-fed mice and were consistent with pathologic angiogenesis. Similarly, it has been

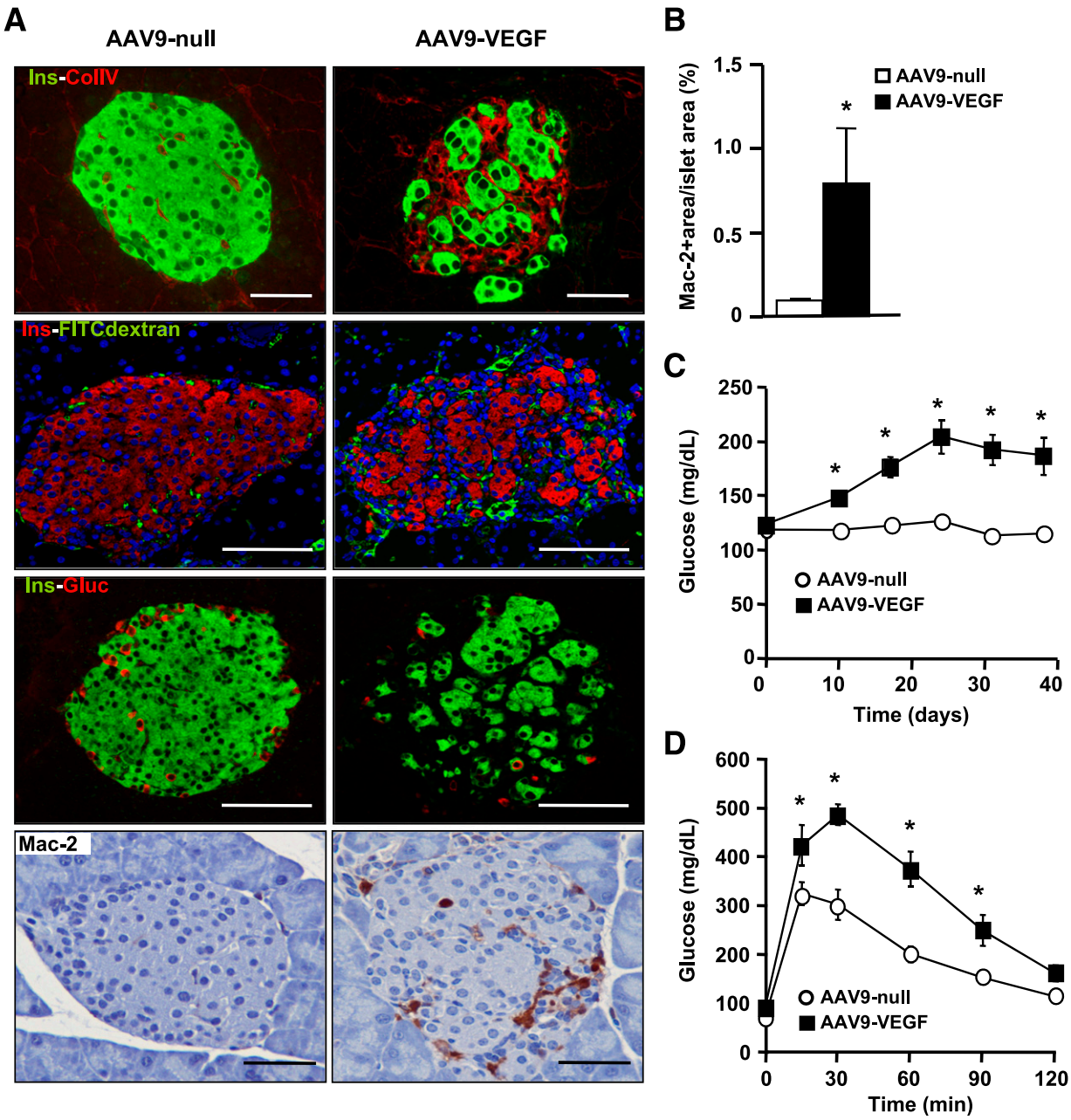

FIG. 7. AAV-mediated VEGF overexpression in β-cells increased islet vascularization and inflammation. Two-month-old wild-type (WT) mice were injected with VEGF-expressing (AAV9-VEGF) or nonexpressing (null) AAV9 vectors (10^{12} vector genomes/mouse). *A*: Ten days after AAV injection vasculature structure was revealed by immunostaining for collagen IV (red) and insulin (green) (*top panel*). VEGF-treated islets showed increased basement membrane compared with AAV-null. FITC-dextran (green) together with insulin (red) immunostaining was used to label functional blood vessels (*top middle panel*). Insulin (green) and glucagon (red) expression showed islet disorganization (*bottom middle panel*). Macrophage infiltration in AAV-VEGF–treated animals was determined by Mac-2 immunostaining 10 days after AAV injection (*bottom panel*). Scale bars, 100 μm. *B*: AAV-VEGF–injected animals showed increased Mac-2–positive area/islet area when compared with AAV-null–treated mice as early as 10 days after injection: AAV-null–treated mice (white bar) and AAV-VEGF–treated mice (black bar) (n = 4 mice/group). *C*: Fed blood glucose levels were determined before AAV injection (day 0) and at several time points thereafter: AAV-null-treated mice (white circle) and AAV-VEGF–treated mice (black square) (n = 10 mice/group). *D*: Glucose tolerance was measured 20 days after AAV administration (2 g/kg body weight) (n = 10 animals/group). *P < 0.05 VEGF vs. null. (A high-quality digital representation of this figure is available in the online issue.)

shown in tumors that prolonged deregulated expression of VEGF leads to aberrant immature vessels that often invade the surrounding tissue (33,34). In contrast, normal vasculature spreads by physiologic angiogenesis, requiring proper regulation of the dose and timing of VEGF production (11,32).

Islets from transgenic $VEGF^{low}$ and $VEGF^{high}$ mice showed thickening of the vessel basal membrane that resulted from increased collagen IV accumulation, which in $VEGF^{high}$ islets disrupted islet structure and was parallel to β-cell loss and development of hyperglycemia. In islets from GK rats, ECM deposition develops from intra- and peri-islet vessels (21,35). The islet ECM is mainly synthesized by endothelial cells, because β-cells do not have an ECM (25,26). Moreover, VEGF is able to induce collagen IV synthesis in cultured endothelial cells (28), which suggests that in islets from VEGF transgenic mice, a VEGF-mediated activation of endothelial cells causes overproduction of ECM components and fibrosis. Similarly, islet fibrosis has

also been described in islets of patients with T2D and in various spontaneous rodent models of T2D, such as *db/db* mice and Zucker and GK rats, in which it is involved in islet destruction (21,36–38). Thus, during T2D, chronic VEGF upregulation in islets may be responsible for ECM accumulation in surrounding islet vessels, leading to fibrosis.

Two-month-old VEGF^{low} and VEGF^{high} mice also displayed disorganized islets with α-cells scattered in the islet core. The Ca^{2+}-dependent cell adhesion molecule E-cadherin, which is highly expressed in pancreatic islets, mediates β-cell-to-β-cell contacts, controlling islet architecture and function (29,30). The expression of E-cadherin was reduced in VEGF^{low} and VEGF^{high} islets, consistent with decreased numbers of direct β-cell-to-β-cell contacts and islet disorganization. It is widely accepted that proper insulin secretion requires the coordinated function of the β-cells that form an islet (29). Moreover, islet disorganization is considered a hallmark of islet dysfunction (39). However, despite altered islet architecture, 2-month-old VEGF^{low} and VEGF^{high} mice displayed normal in vivo insulin release and glucose tolerance. Therefore, these transgenic mice indicate that abnormal islet morphology is not directly responsible for impaired β-cell function. Because the alteration of insulin secretion developed in parallel with the severity of inflammation, our results suggest that islet inflammation, rather than islet disorganization alone, was probably the proximate cause of islet failure.

Although the precise mechanism or more likely multiple mechanisms underlying decreased β-cell mass and function in T2D remain to be elucidated, islets from patients with T2D display an inflammatory process characterized by the presence of immune cell infiltration, inflammatory cytokines, apoptotic cells, and, eventually, fibrosis. VEGF transgenic mice partially recapitulate those processes that occur specifically in the islets without the development of insulin resistance. VEGF is a powerful chemoattractant for macrophages and other leukocytes at the sites of angiogenesis, where these cells play an important role in vessel formation and tissue remodeling (13,40). Islets from HFD-fed mice showed infiltrating macrophages, comparable to those described in islets from several type 2 diabetic animal models and human patients (7,38,41,42). Increased numbers of macrophages are detectable very early in islets, before the onset of diabetes (41). Normoglycemic insulin-resistant HFD-fed mice showed islet macrophage infiltration concomitant with VEGF upregulation. Similarly, islets from both VEGF^{low} and VEGF^{high} mice were progressively infiltrated by macrophages. Moreover, Mac-2^{+} insulitis grade and VEGF upregulation level in VEGF^{low} mice were similar to those observed in prediabetic HFD-fed mice. Finally, VEGF transgenic islets showed macrophage infiltration even before developing impaired glucose homeostasis, suggesting that infiltration is not a consequence of β-cell death. Therefore, this study suggests that macrophage infiltration may already be induced during islet hyperplasia and play a role in initiating and/or accelerating β-cell failure. This hypothesis is supported by the AAV-mediated overexpression of VEGF in islets of adult mice, because, as early as 10 days after vector administration, mice already showed islet disorganization and inflammation, which subsequently progressed to hyperglycemia and glucose intolerance.

VEGF-expressing islets showed macrophage infiltration and increased expression of IL-1β, CCL-2, and TNF-α. A significant increased in cytokine expression was detected at a slightly delayed time compared with macrophage infiltration, but both inflammatory processes increased with age and VEGF levels. Macrophages are able to secrete a broad range of cytokines. In RIP-CCL2 transgenic mice, myeloid cell infiltration of islets is able to induce β-cell death and diabetes (43). Moreover, it has been shown that high glucose concentrations can induce β-cell expression of several cytokines, such as IL-1β and CCL-2 (44–46). Thus, during development of T2D, VEGF and inflammatory cytokines may be secreted and attract macrophages, and, in turn, macrophages can produce higher levels of proinflammatory cytokines. These processes probably stimulate each other in a positive-feedback manner, and, together with other processes such as endoplasmic reticulum (ER) stress, may contribute to β-cell failure and death. During T2D, higher insulin requirements and high circulating levels of free fatty acids and glucose can lead to the activation of the unfolding protein response and ER stress within the β-cells (47). Moreover, several studies have proposed that proinflammatory cytokines are also able to induce β-cell apoptosis by means of ER stress (47–49). Because VEGF overexpression in islets from our transgenic mice resulted in enhanced cytokine production, this may also contribute to β-cell loss through ER stress.

It is of interest that although previous reports demonstrated that decreased VEGF expression in β-cells resulted in insufficient vascularization leading to impaired insulin secretion and glucose intolerance (14), our results suggest that excessive islet VEGF production also triggers architectural abnormalities and impaired β-cell function. Thus, VEGF levels need to be finely and tightly regulated to avoid development of undesirable hypervascularization, fibrosis, and inflammation.

Finally, although no direct links between angiogenic factor genetic variants and diabetes have been reported, allelic variants of VEGF (50) and the VEGF-inducer transcription factor hypoxia inducible factor-1α have been described in T2D patients (51). Moreover, polymorphisms in the VEGF-A gene have been reported in patients with micro and macrovascular diabetic secondary complications (52,53). These data further suggest that dysregulation of VEGF could be involved in the pathogenesis of T2D.

In summary, the current study demonstrates a crucial role for islet vascularization and inflammation in the development of β-cell failure, suggesting that macrophage recruitment and sustained islet cytokine production may result from increased angiogenesis and/or VEGF upregulation and that this inflammatory process may contribute to connect insulin resistance with β-cell death and T2D.

ACKNOWLEDGMENTS

This work was supported by grants from Ministerio de Ciencia e Innovación, Plan Nacional I+D+I (SAF2008-00962) and Generalitat de Catalunya (2009 SGR-224), and Spain and European Commission (EUGENE2, LSHM-CT-2004-512013; CLINIGENE, LSHB-CT-2006-018933). J.A., V.J., C.M., and A.R. were recipients of predoctoral fellowships from Ministerio de Educación and Cultura y Deporte and A.S. from Direcció General de Recerca, Generalitat de Catalunya.

No potential conflicts of interest relevant to this article were reported.

J.A., E.A., V.J., and F.B. designed experiments. J.A., E.A., V.J., A.C., C.M., A.S., S.T., M.O., A.R., M.M., and A.P. generated reagents and performed experiments. J.A. and F.B. wrote and edited the manuscript. F.B. is the guarantor of this work and, as such, had full access to all the data in the study and takes responsibility for the integrity of the data and the accuracy of the data analysis.

The authors thank C.J. Mann, Universitat Pompeu Fabra, S. Franckhauser, Universitat Autònoma Barcelona, and J. Storch, Rutgers University, for helpful discussion.

REFERENCES

1. Mathis D, Vence L, Benoist C. beta-Cell death during progression to diabetes. Nature 2001;414:792–798
2. Rhodes CJ. Type 2 diabetes-a matter of beta-cell life and death? Science 2005;307:380–384
3. Kahn SE, Hull RL, Utzschneider KM. Mechanisms linking obesity to insulin resistance and type 2 diabetes. Nature 2006;444:840–846
4. Sakuraba H, Mizukami H, Yagihashi N, Wada R, Hanyu C, Yagihashi S. Reduced beta-cell mass and expression of oxidative stress-related DNA damage in the islet of Japanese Type II diabetic patients. Diabetologia 2002;45:85–96
5. Butler AE, Janson J, Bonner-Weir S, Ritzel R, Rizza RA, Butler PC. Beta-cell deficit and increased beta-cell apoptosis in humans with type 2 diabetes. Diabetes 2003;52:102–110
6. McGarry JD, Dobbins RL. Fatty acids, lipotoxicity and insulin secretion. Diabetologia 1999;42:128–138
7. Donath MY, Schumann DM, Faulenbach M, Ellingsgaard H, Perren A, Ehses JA. Islet inflammation in type 2 diabetes: from metabolic stress to therapy. Diabetes Care 2008;31(Suppl. 2):S161–S164
8. Weir GC, Marselli L, Marchetti P, Katsuta H, Jung MH, Bonner-Weir S. Towards better understanding of the contributions of overwork and glucotoxicity to the beta-cell inadequacy of type 2 diabetes. Diabetes Obes Metab 2009;11(Suppl. 4):82–90
9. Busch AK, Cordery D, Denyer GS, Biden TJ. Expression profiling of palmitate- and oleate-regulated genes provides novel insights into the effects of chronic lipid exposure on pancreatic beta-cell function. Diabetes 2002;51:977–987
10. Brissova M, Shostak A, Shiota M, et al. Pancreatic islet production of vascular endothelial growth factor—a is essential for islet vascularization, revascularization, and function. Diabetes 2006;55:2974–2985
11. Carmeliet P. Angiogenesis in health and disease. Nat Med 2003;9:653–660
12. Nieves BJ, D'Amore PA, Bryan BA. The function of vascular endothelial growth factor. Biofactors 2009;35:332–337
13. Sawano A, Iwai S, Sakurai Y, et al. Flt-1, vascular endothelial growth factor receptor 1, is a novel cell surface marker for the lineage of monocyte-macrophages in humans. Blood 2001;97:785–791
14. Lammert E, Gu G, McLaughlin M, et al. Role of VEGF-A in vascularization of pancreatic islets. Curr Biol 2003;13:1070–1074
15. Konstantinova I, Lammert E. Microvascular development: learning from pancreatic islets. Bioessays 2004;26:1069–1075
16. Olsson R, Carlsson PO. The pancreatic islet endothelial cell: emerging roles in islet function and disease. Int J Biochem Cell Biol 2006;38:710–714
17. Jabs N, Franklin I, Brenner MB, et al. Reduced insulin secretion and content in VEGF-a deficient mouse pancreatic islets. Exp Clin Endocrinol Diabetes 2008;116(Suppl. 1):S46–S49
18. Toyofuku Y, Uchida T, Nakayama S, et al. Normal islet vascularization is dispensable for expansion of beta-cell mass in response to high-fat diet induced insulin resistance. Biochem Biophys Res Commun 2009;383:303–307
19. Li X, Zhang L, Meshinchi S, et al. Islet microvasculature in islet hyperplasia and failure in a model of type 2 diabetes. Diabetes 2006;55:2965–2973
20. Masuyama T, Komeda K, Hara A, et al. Chronological characterization of diabetes development in male Spontaneously Diabetic Torii rats. Biochem Biophys Res Commun 2004;314:870–877
21. Homo-Delarche F, Calderari S, Irminger JC, et al. Islet inflammation and fibrosis in a spontaneous model of type 2 diabetes, the GK rat. Diabetes 2006;55:1625–1633
22. Ko SH, Kwon HS, Kim SR, et al. Ramipril treatment suppresses islet fibrosis in Otsuka Long-Evans Tokushima fatty rats. Biochem Biophys Res Commun 2004;316:114–122
23. Nakamura M, Kitamura H, Konishi S, et al. The endocrine pancreas of spontaneously diabetic db/db mice: microangiopathy as revealed by transmission electron microscopy. Diabetes Res Clin Pract 1995;30:89–100
24. Otonkoski T, Banerjee M, Korsgren O, Thornell LE, Virtanen I. Unique basement membrane structure of human pancreatic islets: implications for beta-cell growth and differentiation. Diabetes Obes Metab 2008;10(Suppl. 4):119–127
25. Nikolova G, Jabs N, Konstantinova I, et al. The vascular basement membrane: a niche for insulin gene expression and Beta cell proliferation. Dev Cell 2006;10:397–405
26. Nikolova G, Strilic B, Lammert E. The vascular niche and its basement membrane. Trends Cell Biol 2007;17:19–25
27. Ayuso E, Mingozzi F, Montane J, et al. High AAV vector purity results in serotype- and tissue-independent enhancement of transduction efficiency. Gene Ther 2010;17:503–510
28. Infanger M, Grosse J, Westphal K, et al. Vascular endothelial growth factor induces extracellular matrix proteins and osteopontin in the umbilical artery. Ann Vasc Surg 2008;22:273–284
29. Rogers GJ, Hodgkin MN, Squires PE. E-cadherin and cell adhesion: a role in architecture and function in the pancreatic islet. Cell Physiol Biochem 2007;20:987–994
30. Jain R, Lammert E. Cell-cell interactions in the endocrine pancreas. Diabetes Obes Metab 2009;11(Suppl. 4):159–167
31. Jimenez V, Ayuso E, Mallol C, et al. In vivo genetic engineering of murine pancreatic beta cells mediated by single-stranded adeno-associated viral vectors of serotypes 6, 8 and 9. Diabetologia 2011;54:1075–1086
32. Carmeliet P. Angiogenesis in life, disease and medicine. Nature 2005;438:932–936
33. Carmeliet P. VEGF as a key mediator of angiogenesis in cancer. Oncology 2005;69(Suppl. 3):4–10
34. van Beijnum JR, Petersen K, Griffioen AW. Tumor endothelium is characterized by a matrix remodeling signature. Front Biosci (Schol Ed) 2009;1:216–225
35. Lacraz G, Giroix MH, Kassis N, et al. Islet endothelial activation and oxidative stress gene expression is reduced by IL-1Ra treatment in the type 2 diabetic GK rat. PLoS ONE 2009;4:e6963
36. Portha B, Lacraz G, Kergoat M, et al. The GK rat beta-cell: a prototype for the diseased human beta-cell in type 2 diabetes? Mol Cell Endocrinol 2009;297:73–85
37. Tal MG. Type 2 diabetes: Microvascular ischemia of pancreatic islets? Med Hypotheses 2009;73:357–358
38. Ehses JA, Böni-Schnetzler M, Faulenbach M, Donath MY. Macrophages, cytokines and beta-cell death in Type 2 diabetes. Biochem Soc Trans 2008;36:340–342
39. Shih DQ, Heimesaat M, Kuwajima S, Stein R, Wright CV, Stoffel M. Profound defects in pancreatic beta-cell function in mice with combined heterozygous mutations in Pdx-1, Hnf-1alpha, and Hnf-3beta. Proc Natl Acad Sci USA 2002;99:3818–3823
40. Soucek L, Lawlor ER, Soto D, Shchors K, Swigart LB, Evan GI. Mast cells are required for angiogenesis and macroscopic expansion of Myc-induced pancreatic islet tumors. Nat Med 2007;13:1211–1218
41. Ehses JA, Perren A, Eppler E, et al. Increased number of islet-associated macrophages in type 2 diabetes. Diabetes 2007;56:2356–2370
42. Grunnet LG, Aikin R, Tonnesen MF, et al. Proinflammatory cytokines activate the intrinsic apoptotic pathway in beta-cells. Diabetes 2009;58:1807–1815
43. Martin AP, Rankin S, Pitchford S, Charo IF, Furtado GC, Lira SA. Increased expression of CCL2 in insulin-producing cells of transgenic mice promotes mobilization of myeloid cells from the bone marrow, marked insulitis, and diabetes. Diabetes 2008;57:3025–3033
44. Maedler K, Sergeev P, Ris F, et al. Glucose-induced beta cell production of IL-1beta contributes to glucotoxicity in human pancreatic islets. J Clin Invest 2002;110:851–860
45. Maedler K, Størling J, Sturis J, et al. Glucose- and interleukin-1beta-induced beta-cell apoptosis requires Ca2+ influx and extracellular signal-regulated kinase (ERK) 1/2 activation and is prevented by a sulfonylurea receptor 1/inwardly rectifying K+ channel 6.2 (SUR/Kir6.2) selective potassium channel opener in human islets. Diabetes 2004;53:1706–1713
46. Jonas JC, Bensellam M, Duprez J, Elouil H, Guiot Y, Pascal SM. Glucose regulation of islet stress responses and beta-cell failure in type 2 diabetes. Diabetes Obes Metab 2009;11(Suppl. 4):65–81
47. Kharroubi I, Ladrière L, Cardozo AK, Dogusan Z, Cnop M, Eizirik DL. Free fatty acids and cytokines induce pancreatic beta-cell apoptosis by different mechanisms: role of nuclear factor-kappaB and endoplasmic reticulum stress. Endocrinology 2004;145:5087–5096
48. Tersey SA, Nishiki Y, Templin AT, et al. Islet β-cell endoplasmic reticulum stress precedes the onset of type 1 diabetes in the nonobese diabetic mouse model. Diabetes 2012;61:818–827
49. Cardozo AK, Ortis F, Storling J, et al. Cytokines downregulate the sarcoendoplasmic reticulum pump Ca2+ ATPase 2b and deplete endoplasmic reticulum Ca2+, leading to induction of endoplasmic reticulum stress in pancreatic beta-cells. Diabetes 2005;54:452–461
50. Lu F, Qian Y, Li H, et al. Genetic variants on chromosome 6p21.1 and 6p22.3 are associated with type 2 diabetes risk: a case-control study in Han Chinese. J Hum Genet 2012;57:320–325
51. Yamada N, Horikawa Y, Oda N, et al. Genetic variation in the hypoxia-inducible factor-1alpha gene is associated with type 2 diabetes in Japanese. J Clin Endocrinol Metab 2005;90:5841–5847
52. Tavakkoly-Bazzaz J, Amoli MM, Pravica V, et al. VEGF gene polymorphism association with diabetic neuropathy. Mol Biol Rep 2010;37:3625–3630
53. Chun MY, Hwang HS, Cho HY, et al. Association of vascular endothelial growth factor polymorphisms with nonproliferative and proliferative diabetic retinopathy. J Clin Endocrinol Metab 2010;95:3547–3551